The Annual Cycle over the Tropical Atlantic, South America, and Africa[*]

M. Biasutti, D. S. Battisti, and E. S. Sarachik

Department of Atmospheric Sciences, University of Washington, Seattle, Washington

ABSTRACT

The annual cycle over land can be thought of as being forced locally by the direct action of the sun and remotely by circulations forced by regions of persistent precipitation organized primarily by SST and, secondarily, by land. This study separates these two sources of annual variability in order to indicate where and when the remote effects are important.

Two main sets of AGCM experiments were performed: one with fixed SST boundary conditions and seasonally varying insolation, another with fixed insolation and seasonally varying SST. For each experiment, the evolution of the annual cycle is presented as the differences from the reference month of March. The comparison of other months to March in the fixed-SST runs separates out the direct response of the land–atmosphere system to the annual insolation changes overhead. Similarly, the same comparison in the annual cycle of the fixed-insolation runs reveals the response of the land–atmosphere system to changes in SST.

Over most of the domain, insolation is the dominant forcing on land temperature during June and December, but SST dominates during September. Insolation determines the north–south displacement of continental convection at the solstices and greatly modulates the intensity of precipitation over the tropical Atlantic Ocean.

The SST determines the location of the ITCZ over the oceans and influences continental precipitation in coastal regions and in the Sahel/Sudan region. In September, when SST deviations from the March reference values are largest, the SST influence on both precipitation and surface air temperature extends to most of the tropical land. SST is an important forcing for the surface air temperature in the Guinea highlands and northeast Brazil throughout the year.

1. Introduction

A number of short-term climate forecast techniques have recently been developed for specific land regions of the Tropics, in particular northeast Brazil (e.g., Folland et al. 2001) and the Sahel (e.g., Ward 1998). These techniques are based on proven interannual (or longer) correlations of global sea surface temperature (SST) with air temperature and precipitation in the given regions. These correlations are hard won [e.g., Folland et al. (1986) for the Sahel and Uvo et al. (1998) for northeast Brazil], since long time series are needed to gather the statistics of SST anomalies from the annual cycle and of local temperature and precipitation anomalies. Yet there is no process in the atmosphere on these longer timescales that does not also act on the shorter annual timescale. The difficulty, of course, is that everything varies annually so that perfect correlations tell us nothing about what SST does and does not influence.

Corresponding author address: Michela Biasutti, JISAO, University of Washington, Box 354235, Seattle, WA 98195-4235.
E-mail: biasutti@atmos.washington.edu

The annual cycle over land can be thought of as being forced locally by the direct action of the sun and remotely by circulations forced by regions of persistent precipitation organized primarily by SST and, secondarily, by land. This distinction can be applied to monsoon regions as well, because the reversal of land–sea temperature gradients that drives the monsoon is determined primarily by land temperature changes, and therefore primarily by insolation. If local and remote sources of annual variability could be separated, then where and when the remote effects of SST are important could be quantified simply by decomposing and analyzing the annual cycle.

This separation clearly cannot be done observationally, but can be done in atmospheric models of the annual cycle. Thus, Shukla and Fennessy (1994) investigated the Asian summer monsoon in a set of 6-month-long AGCM simulations with seasonally varying SST and insolation, fixed SST and seasonally varying insolation, and seasonally varying SST and fixed insolation; they concluded that the annual cycle of SST is just as important as the annual cycle of solar forcing in the establishment of the summer Asian monsoon. Li and Philander (1997), using an atmospheric GCM forced by specified SST, suppressed the annual cycle of SST by replacing it with an unchanging annual mean while leav-

ing the annual solar variation untouched. They found that even over the unchanging ocean in the Gulf of Guinea, an annual cycle of the model meridional winds could be induced by the annual variation of temperature over land forced locally by the annual cycle of solar heating. Similarly Fu et al. (2001) selectively suppressed the annual cycle of SST in different regions to examine effects of SST on precipitation in the Amazon basin.

We concentrate on the Atlantic because there the annual cycle is relatively pure: internal variability is small compared to annual variability (Carton and Zhou 1997) and occurs mostly on decadal timescales. In the Pacific, by contrast, a good deal of the annual cycle is due to averaging of mostly longer-term ENSO variability that is tied to the annual cycle. Moreover, the effect of SST variations over Africa and South America has generated a lot of interest in recent years. Besides in the seasonal predictability studies mentioned above, land–sea interactions in the Atlantic regions have been deemed important in studies of decadal variability (e.g., Nobre and Shukla 1996; Rowell et al. 1995; Eltahir and Gong 1996; Werner 1999), and paleomonsoons (e.g., Braconnot et al. 2000).

We use a standard atmospheric general circulation model, version 3 of the National Center for Atmospheric Research (NCAR) Community Climate Model (CCM3) [this is essentially the same model used by Fu et al. (2001) except that, in that work, the land model was replaced by a different model]. We use the model in its original form (Kiehl et al. 1998) whose annual cycle was extensively evaluated by comparing a 15-yr simulation forced by observed SST to observations (Hurrell et al. 1998; Bonan 1998).

Because Bonan (1998) evaluated the global aspects of the model without much attention to the Atlantic, and because Fu et al. (2001) evaluated the model only in the Amazon region, we will reexamine the capabilities of the model to simulate the annual cycle in the Atlantic region (Fig. 1), comprising the tropical Atlantic, South America, and Africa.

We then use the model in a manner similar to Li and Philander (1997) but, instead of specifying an unchanging mean SST, we specify constant values of SST at various phases of the annual cycle and allow the sun to vary through its annual cycle. To complete the separation, we specify constant values of the sun at two (extreme) phases of its annual cycle and allow the SST to vary annually. This separation of local and remote effects allows us to estimate not only where SST is important, but also when.

In summary, the objective of this paper is to study the *atmospheric response* to the specified annual cycle of both ocean boundary conditions and radiative forcing. This decomposition will provide a first-order indication of how the annual cycle is set, but it obviously neglects some important physics of the coupled system: the effects of thermodynamic and dynamic ocean–atmosphere coupling and of nonlinearities in the coupled
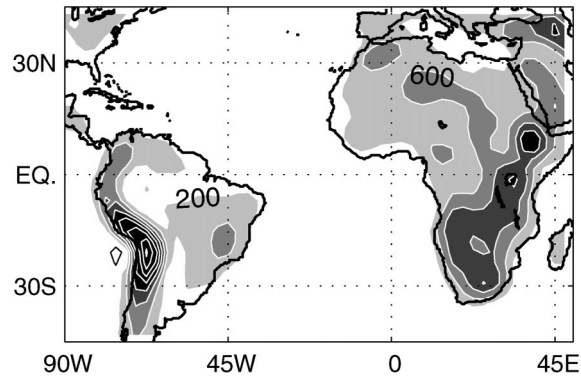

FIG. 1. The region of interest and its orography at T42 resolution. The contour interval is 400 m, starting at the −200-m value. (Negative altitudes of −200 m—due to Gibbs fringes—are contoured in black, barely visible west of the Andes.) At T42 resolution the highest peak in the Andes is 3000 m high.

system have been consciously overlooked. Therefore, our analysis is not complete. While the effect of SST on land is totally taken into account, the effect of land on SST is necessarily neglected by the artifice of specifying the SST. This might be particularly problematic for the annual cycle in the equatorial waveguide region, where air–sea interaction determines the behavior of the ITCZ–cold tongue complex (see, e.g., Mitchell and Wallace) 1992; Xie and Philander 1994; Philander et al. 1996).

This paper is organized as follows. In section 2 we introduce the model and validate the control climatology against observations and the National Centers for Environmental Prediction (NCEP) reanalysis. In section 3 we describe the experiments performed, and in section 4 we comment on the simulated annual cycles. In sections 5 and 6 we present our main results, namely, the response of the AGCM to SST and to insolation changes, respectively. In section 7 we discuss the statistical significance of the responses and also indicate where SST and insolation interact in a nonlinear fashion to produce the simulated seasonal cycle. In section 8 we summarize our main results, present the implications for variability studies, and offer some caveats in the interpretation of our results.

2. The model

The model used in this study is the CCM3 developed at NCAR, run at the standard resolution T42L19 (triangular spectral truncation at wavenumber 42, corresponding to a grid about 2.8° × 2.8°; and 19 mixed sigma and pressure vertical levels). The NCAR Land Surface Model (LSM; Bonan 1996) is coupled to the atmospheric component to simulate the effect of vegetation and soil hydrology on land–atmosphere exchanges (Bonan 1998). A detailed description of the model, its dynamical core, its physical parameterizations, and its overall performance, can be found in Kiehl

et al. (1998), Hack et al. (1998), Bonan (1998), and other papers in the same special issue of *Journal of Climate* (1998, Vol. 11, no. 6). Fu et al. (2001) have used the same atmospheric model, but coupled to a different land surface model [the Biosphere–Atmosphere Transfer Scheme (BATS); Dickinson et al. 1993], to determine how SST influences precipitation in the equatorial Amazon, and found that the model qualitatively agrees with observations, and is therefore suitable for this kind of experiment.

We compare precipitation, surface air temperature, and surface winds simulated by the control run (CTL) with those observed [the Global Precipitation Climatology Project (GPCP) precipitation product; Huffman et al. (1997)] or produced by the NCEP–NCAR reanalysis project [for surface air temperature and wind; Kalnay et al. (1996)]. Note that the observed and reanalyzed climatologies refer to different time periods, and that the CTL climatology is obtained from a run with climatological SST boundary conditions (Shea et al. 1992), themselves different from the ones used by the reanalysis (Reynolds and Smith 1994; Parker et al. 1996). Therefore, in-detail agreement should not be expected.

Figure 2 compares the reanalyzed and simulated March, June, September, and December surface air temperature. The differences over the ocean are consistent with the discrepancies in the SST products noted above. Over the continents the temperature pattern is quite similar to that observed, and the progression of the annual cycle is well simulated. This consistency goes beyond the obvious cooling in the winter and warming in the summer, and can be found in some of the spatial details. For example, over northern Africa the isotherms are quite zonal in March, but a localized maximum confined to western Africa develops in June; in the Amazon basin a temperature maximum develops in September. Nevertheless, the model has a substantial cold bias throughout the year in the Sahara Desert [because the soil albedo is too high, as reported by Bonan (1998)], Chile and Argentina, and—to a lesser degree—South Africa. A warm bias is present in the Amazon basin during austral winter and spring.

Figure 3 compares observed rainfall and reanalyzed surface winds with the CTL simulation. The CCM reproduces fairly well the seasonal movement of the ITCZ and the succession of dry and wet seasons over the continents. The agreement is less satisfactory when we compare the mean precipitation, instead of the seasonal changes. The CCM exhibits a substantial bias over central equatorial Africa, where it produces twice the observed precipitation all year-round, and in the mountainous regions of southern Africa and South America (wet bias during March and December). In general the ITCZ is displaced somewhat too far to the south, and the Caribbean region is too wet during boreal summer and fall. While the wet bias in the equatorial and southwestern Africa is a shortcoming specific to the CCM,

the other biases (position of the ITCZ, orographic effect over the Andes during the summer months, and the wet Caribbean) are shared with the NCEP reanalysis (not shown). The fact that a model simulation (i.e., the reanalysis) constrained to be close to the observed circulation produces errors in the rainfall field similar to those seen in the CCM suggests that such common biases are due to the inadequate representation of convection in current GCMs, and that the CCM is otherwise capable of producing a realistic large-scale circulation. Figure 3 shows that the low-level circulation is in fact satisfactory, aside from the exaggerated strength of the wind over the Sahara and in southern Africa: the local orography (Fig. 1) is not properly represented at the T42 resolution, and does not constitute an efficient barrier to the moist wind blowing into Africa from the Indian Ocean. Most likely, the excessive moisture thus spuriously imported into Africa causes the excessive precipitation.

In summary, the CCM reproduces fairly well the main patterns of the seasonal evolution of temperature and precipitation in the tropical Atlantic, South America, and Africa, but presents substantial biases in the amount of continental precipitation. Thus, our model results can be applied to the annual cycle in the real world only as long as no pretense is made of explaining the subtleties of the observed climatology. In particular, we caution the reader about the risk that the effect of continental precipitation might be exaggerated in our study, due to the conspicuous wet bias of the model over equatorial South America and Africa.

3. Experimental design

The main purpose of this study is to separate the response of the climate of the Atlantic Ocean and of Africa and South America to local and remote forcings on the annual timescale. For the tropical landmasses, the local annual forcing comes, to zeroth order, from the insolation overhead; and the remote annual forcing comes, via the atmospheric circulation, from the annual cycle of SST that organizes the oceanic convective centers. An analogous decomposition applies to the case of the ocean. A way to separate the local and remote response is, therefore, to run a set of experiments in which only one of the two annual forcings is present (either the annual cycle of SST or the annual cycle of insolation), and to investigate the response to such forcing over both the oceanic and the continental regions.

Table 1 gives a brief reference for the experiments presented in this paper. We ran a control simulation (CTL), four main experiments (PMS, PSS, PVE, and PWSol) and two additional experiment (PMAS, PM). In the first two experiments, insolation cycles through the annual climatology, while the SST is kept fixed either to the March value [perpetual March SST (PMS)] or to the September value [perpetual September SST (PSS)]. In the second two experiments, conditions are
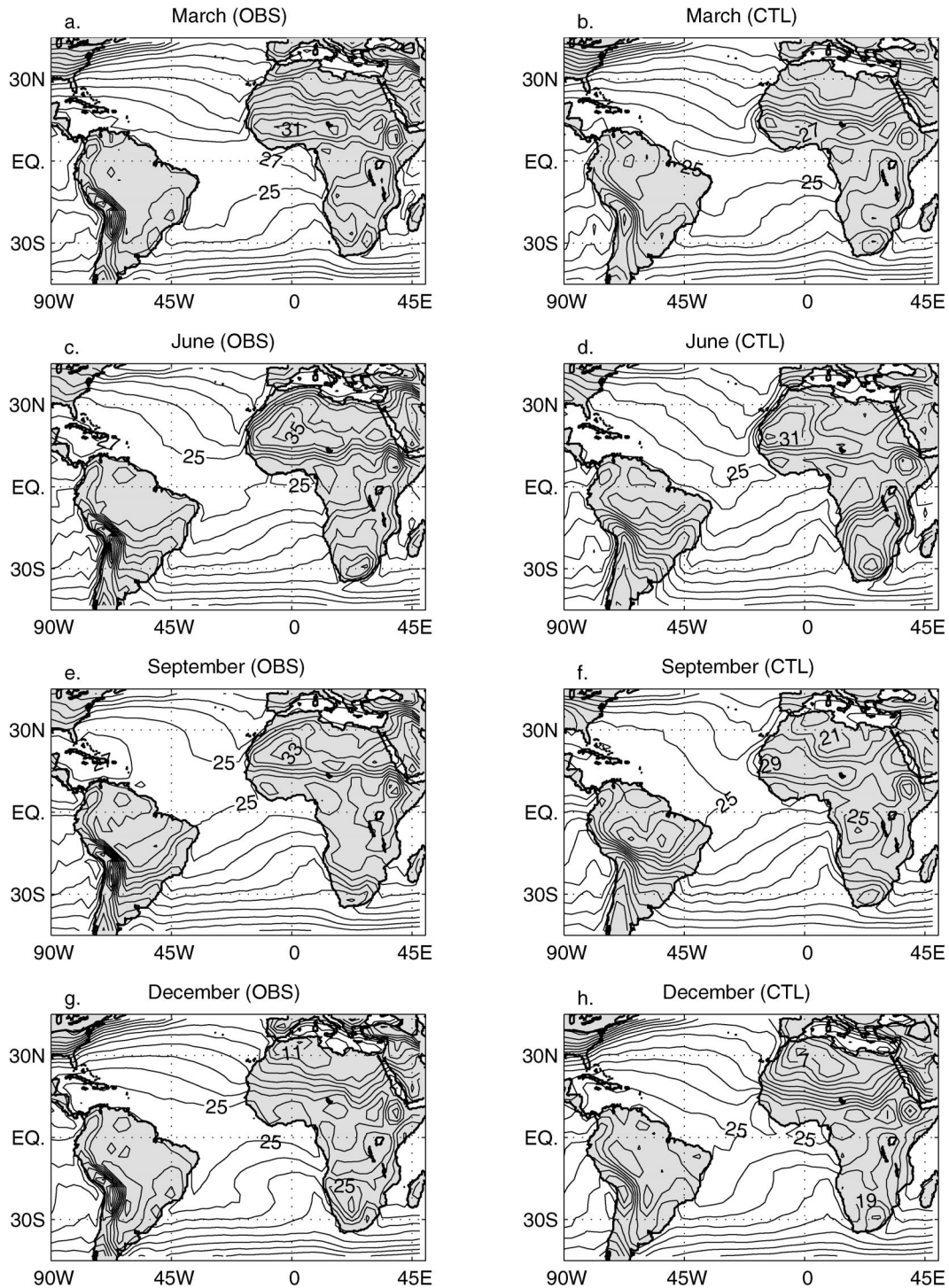
FIG. 2. Climatological annual cycle of surface air temperature in the (a), (c), (e), (g) NCEP reanalysis (OBS) and (b), (d), (f), (h) the control run (CTL). All fields are regridded to the T42 grid. "Surface" is defined as the 0.995 sigma level in the NCEP model, and as the 0.992 sigma level in CCM. The contour interval is 2°C. The CTL run reproduces quite well the evolution of the annual cycle, although it consistently underestimates continental temperatures.
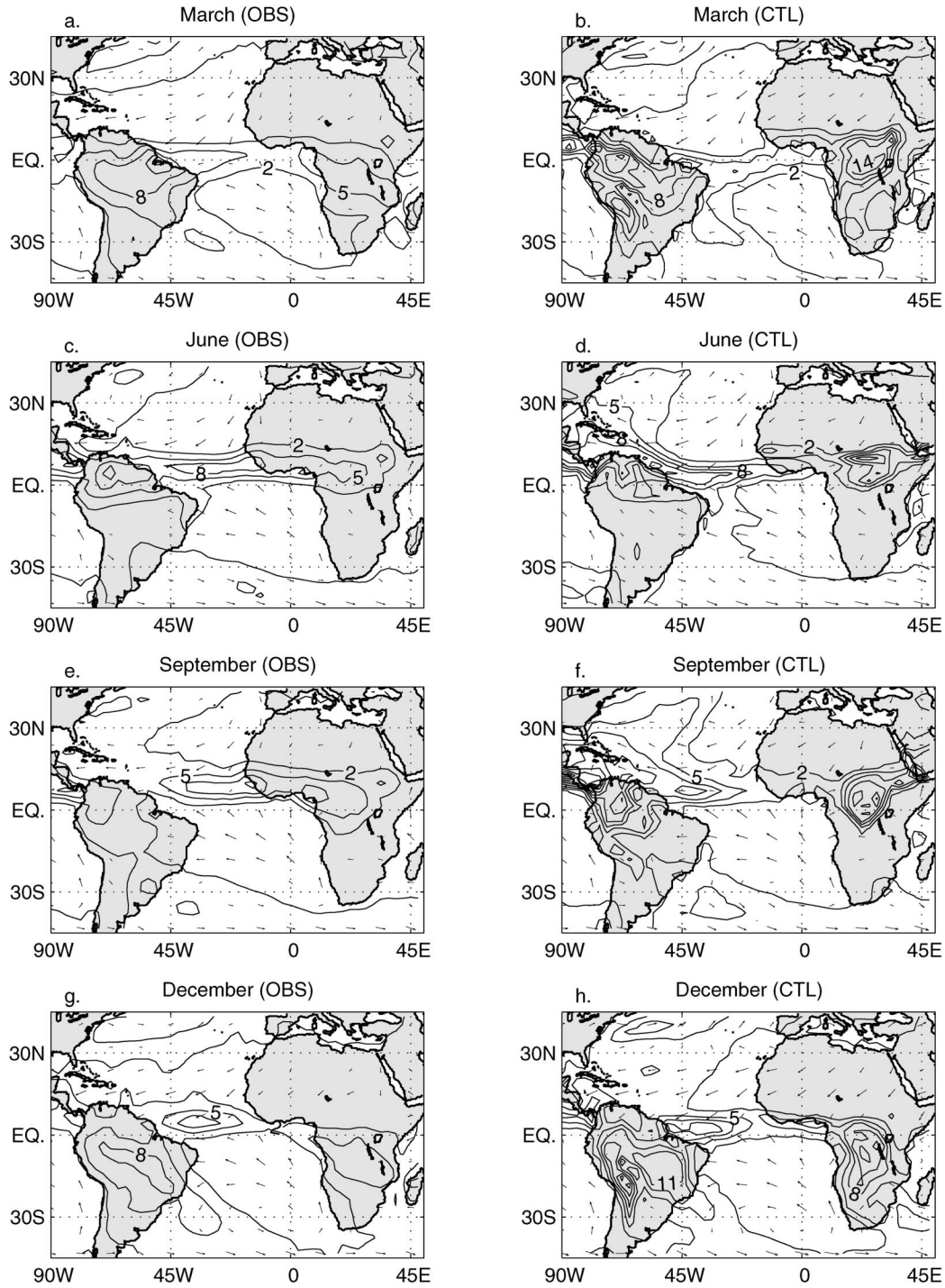
FIG. 3. Climatological annual cycle of precipitation and surface wind (a), (c), (e), (g) in the GPCP dataset and NCEP reanalysis, respectively (OBS), and (b), (d), (f), (h), in the control run (CTL). All fields are regridded to the T42 grid. Surface is defined as the 0.995 sigma level in the NCEP model, and as the 0.992 sigma level in CCM. The contour interval for precipitation is 3 mm day^{-1}, starting with the 2 mm day^{-1} contour. The smallest arrow plotted corresponds to a 2 m s^{-1} wind. The CTL run reproduces quite well the evolution of the annual cycle, although it consistently overestimates African rainfall, and displaces the ITCZ to the south.

TABLE 1. List of experiments: name, insolation forcing, SST boundary conditions, and interpretation.

Name	Insolation	SST	Month to month changes are due to seasonal changes in the following:
CTL	Climatological	Climatological SST	Insolation and SST (Fig. 6)
PMS	Climatological	Perpetual Mar SST	Insolation only (Figs. 9–10)
PSS	Climatological	Perpetual Sep SST	
PVE	Perpetual vernal equinox	Climatological SST	SST only (Figs. 7–8)
PWSol	Perpetual winter solstice	Climatological SST	
PMAS	Climatological	Perpetual Mar Atlantic SST (climatological SST elsewhere)	Insolation and SST everywhere *except* in the Atlantic (not shown)
PM	Perpetual vernal equinox	Perpetual Mar SST	N/A (not shown)

reversed: SST cycles through its annual climatology, while the insolation is kept fixed either to the boreal spring equinox value [perpetual vernal equinox (PVE)] or to the boreal winter solstice value [perpetual winter solstice (PWSol)[1]]. In the fifth experiment [perpetual March Atlantic SST (PMAS)] both the insolation and the Pacific and Indian SSTs are allowed to vary according to their climatology, and only the SST in the Atlantic is held fixed at the March value. We will not show the PMAS simulation, but we will use results from it as an aid for the interpretation of the main experiments. In all these cases we ran the CCM for at least 8 yr and disregarded the first few years, in which the model had not yet fully reached equilibrium. The last experiment is a perpetual March experiment (PM; with perpetual vernal equinox insolation and perpetual March SST boundary conditions). The PM will only be used in section 7 (in conjunction with PVE, PMS, and CTL) to measure the statistical significance of our results. Table 1 provides a reference for the interpretation of each run, and lists the relevant figures.

Instead of presenting the annual cycle as an anomaly from the annual mean, we present it as changes from a single reference month, namely, March (note that we will refer to the ''differences from the reference month March'' as to ''anomalies''). The only reason for this choice is that it makes the discussion in the next sections more effective, but any other method to describe the evolution of the annual cycle, such as differences from any other reference month or from the annual mean, would be equivalent. For example, the temperature difference June − March in the PMS run will give us an estimate of the amount of March to June seasonal change that can be ascribed solely to the corresponding changes in insolation. Similarly, the temperature difference June − March in the PVE run estimates the change ascribable solely to changes in SST.

In sections 5 and 6 we will refer to such seasonal changes as to the ''portion'' of the annual cycle due to each individual forcing. Yet, the reader should keep in mind that these ''portions'' do not add up linearly to the full control annual cycle. Moreover, because the climate system is nonlinear and has long-term memory, the response to the same prescribed forcing may be different when the forcing is applied to a different basic state. Therefore, estimates of the response to insolation changes or SST changes can be different for different experiments. For example, the difference June(PMS) − March(PMS) estimates the effect of insolation in a world with perpetual March SST, while June(PSS) − March(PSS) estimates the same quantity, but for a world with perpetual September SST. The two estimates turn out to be somewhat different (see section 6). Similar considerations apply for the case of the PVE run (from which we can infer the effect of SST under perpetual boreal spring insolation) and the PWSol run (from which we can infer the effect of SST under perpetual boreal winter insolation). In the next sections we will present the different estimates and comment on their differences and the effect of nonlinearities, but will focus mostly on those structures that are more robust.

4. On the simulated climatologies

a. Comments on the fixed-boundary-condition runs

Because the memory of the land–atmosphere system is longer than a month, the climate of any given month is dependent upon the history of the system in the previous months. Therefore, March (PMS) and March (PVE) can be expected to differ from March (CTL), and similarly, September (PSS) and December (PWSol) should differ from September (CTL) and December (CTL). Figures 4 and 5 show how important this effect is on surface air temperature and precipitation, respectively.

As expected, temperature effects are virtually limited to the land, where the soil maintains its memory from one month to the next via its moisture content. Over the ocean, air temperature is a ''slave'' to SST and the memory of the system is artificially suppressed in an AGCM run. As a result, SAT anomalies over the ocean are quite closely confined to coastal regions (although, in the PWSol run, wintertime advection from the cold continent makes them reach as far as 45°W in the North

---

[1] In the PVE and PWSol runs, the phenology of the vegetation describing the leaf and stem area is also held fixed at the March and December values, respectively. Note that we have verified that an experiment with fixed vernal equinox insolation and annually varying phenology gave results virtually indistinguishable from those obtained from the PVE run.
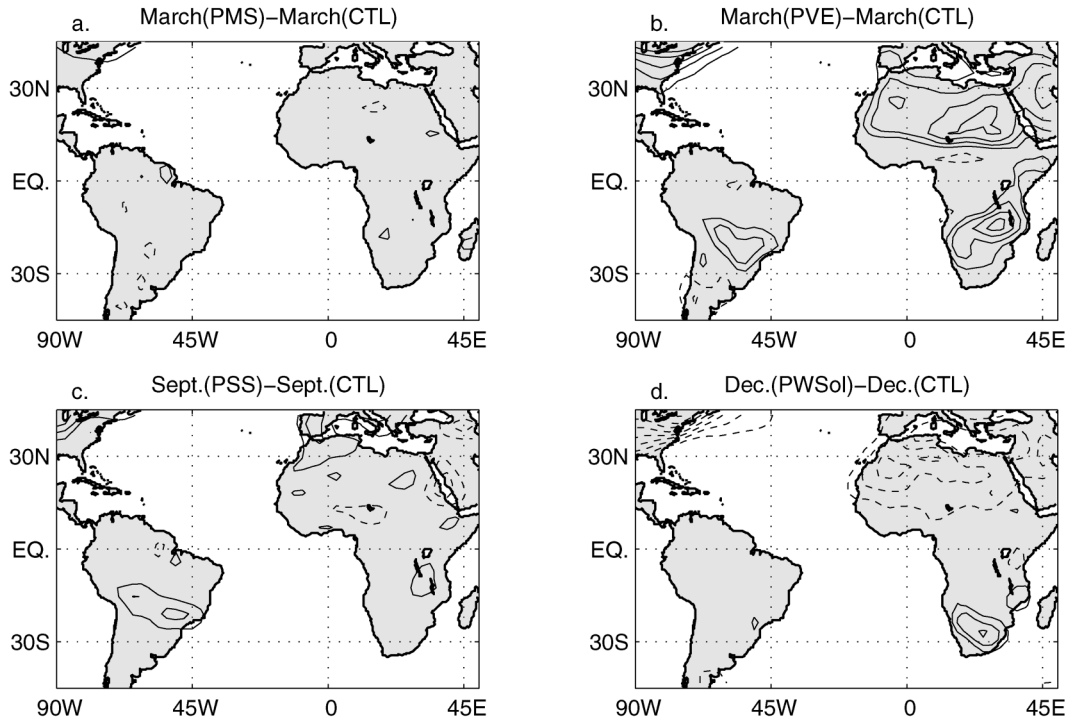
a.   March(PMS)−March(CTL)

b.   March(PVE)−March(CTL)

c.   Sept.(PSS)−Sept.(CTL)

d.   Dec.(PWSol)−Dec.(CTL)

FIG. 4. SAT anomalies from the CTL run: (a) Mar(PMS) − Mar(CTL); (b) Mar(PVE) − Mar(CTL); (c) Sep(PSS) − Sep(CTL); (d) Dec(PWSol) − Dec(CTL). The contour interval is 1°C in all panels; the zero contour is omitted. The memory inherent in land surface properties records the history of the forcing, so that having the same forcing of the CTL run during a specific month does not ensure the same climate for that month. SAT anomalies in the fixed insolation runs reflect differences in annual mean insolation.

Atlantic). The surface air temperature anomalies due to fixed insolation are a reflection of the change in annual mean insolation: March insolation is up to 20 W m^{-2} larger than the annual average in the Tropics, and December insolation is 50–150 W m^{-2} less (more) than the annual average in the northern (southern) Tropics. The surface air temperature anomalies due to fixed SST conditions are much smaller than those due to fixed insolation, because in the former case the effect is only indirect, via the changes in circulation and precipitation associated with SST.

In contrast, changes in precipitation (Fig. 5) are not confined to the continents, but extend into the Caribbean Sea and the equatorial Atlantic Ocean, and their magnitude is comparable to that of continental anomalies. Over land, anomalies are a response to changes in low-level stability and soil moisture; over the ocean they are a dynamical response.

Finally, we wish to point out that the equilibrium states in the four experiments do not inordinately diverge from a "reasonable" climate. If, for example, evaporation exceeded precipitation over a certain land region during March, a run with perpetual March forcing would reach equilibrium by drying the soil out in that region. It turns out that these conditions are not met in any of the experiments, and the simulated annual mean soil moisture falls in every case within the range seen

in the control climatology (not shown). Still, each run equilibrates to a different annual mean soil moisture content and surface temperature, and such differences can account for some of the nonlinearities that will be discussed in the next sections.

b. The annual cycle of the control run

The CTL run shows the combined climate response to seasonal changes in both SST and insolation, thus providing a reference against which one can separately compare the anomalies due to SST and those due to insolation. Figure 6 shows the anomalies with respect to March values of surface air temperature and precipitation in the CTL run, an alternate view of Figs. 2b,d,f,h and 3b,d,f,h. In addition, the rightmost panel shows the anomalies from the March value of the zonally averaged boundary conditions: insolation at the top of the atmosphere and SST (which has been zonally averaged in the Atlantic basin only). The SST anomalies are strongest in September and are always positive in most of the northern part of the domain (north of about 5°N), and negative in the southern part. The insolation anomalies are weak in September (with the Northern Hemisphere receiving a slightly higher insolation than in March), and 4 times as large—and, of course, of dif-
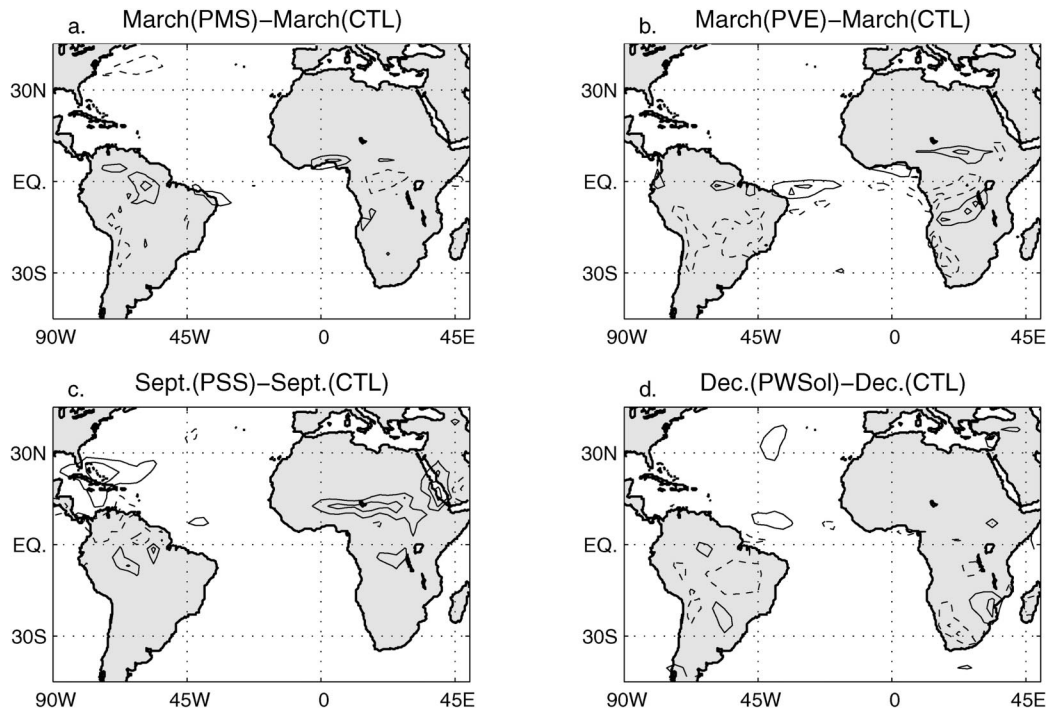
FIG. 5. Rainfall anomalies from the CTL run: (a) Mar(PMS) − Mar(CTL); (b) Mar(PVE) − Mar(CTL); (c) Sep(PSS) − Sep(CTL); (d) Dec(PWSol) − Dec(CTL). The contour interval is 2 mm day^{-1} in all panels; the zero contour is omitted. The memory inherent in land surface properties records the history of the forcing, so that having the same forcing of the CTL run during a specific month does not ensure the same climate for that month.

ferent signs—in the two solstice months, June and December.

Temperature anomalies over land have mostly the sign expected from the insolation anomalies, suggesting that insolation is the dominant forcing. On the other hand, two features suggest that SST must play a nonnegligible role on land surface temperature: (i) the December temperature anomalies are much smaller than those of June (cf. Figs. 6a and 6e), even though the insolation forcing is of equal magnitude; and (ii) in September, between 15°N and 15°S, the temperature anomalies over land in Africa and South America have signs opposite to those of the solar forcing anomalies. [Note that while (i) holds true in observations (not shown), (ii) is true only in South America and not in Africa, where anomalies are slightly negative. Surface air temperature anomalies in the model are too strongly positive; they are associated with excessive negative precipitation anomalies and consequently excessive reduction in latent heat loss.]

Figures 6b,d,f show the annual cycle of precipitation and indicate that, as expected, the ITCZ moves following the warmest waters, and is at its southernmost position during March. Over land, precipitation anomalies have a more complicated structure, but the general picture is of positive anomalies to the north and negative anomalies to the south during June and September, and the opposite during December. This pattern is consistent with continental precipitation following the maximum in insolation.

The modeling results presented in the next two sections support the conclusions suggested above, and evidence a more complex relationship between continental and oceanic precipitation that is not readily visible from the analysis of the annual cycle in the control run.

5. The effect of SST

Figure 7 shows the portion of the annual cycle of surface air temperature that can be attributed solely to changes in SST. In Figs. 7a–f two different estimates are mapped—obtained from the PVE and PWSol run—of the surface air temperature (SAT) response to the evolution of seasonal SST anomalies; the zonal average of the final SST anomaly is shown in the third column. For example, Fig. 7a shows the June–March SAT difference in the PVE run. In this case June and March are distinguished only by the value of the SST boundary condition, because the insolation is kept fixed at the vernal equinox value; therefore, their difference indicates the response to June–March SST. Figure 7b shows the same quantity, but for a run with a different basic state: a different model world, with perpetual winter insolation. The June–March SST (zonally averaged in the Atlantic domain) responsible for both these anomalies is plotted in the last column.
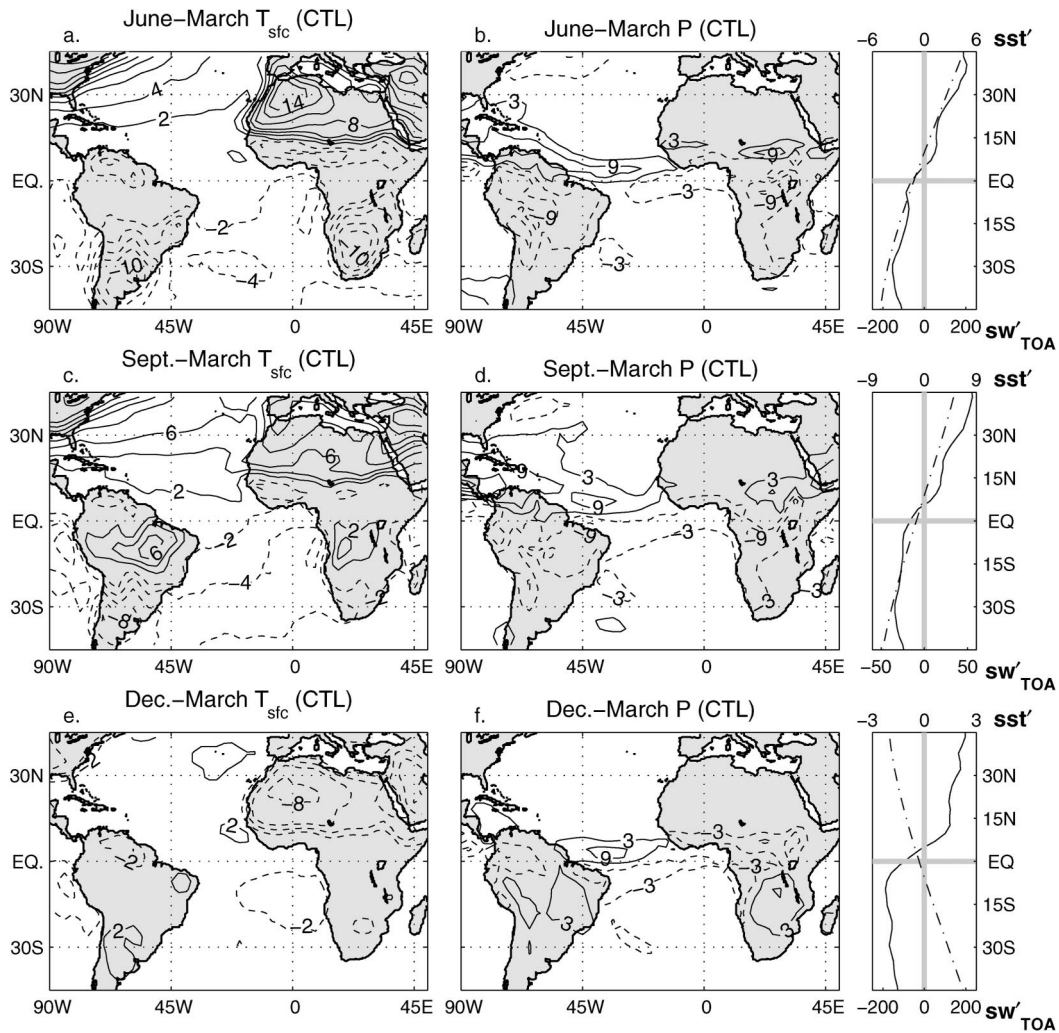
FIG. 6. The annual cycle of the CTL run, presented as departures from the month of March. (a), (c), (e) Surface air temperature (contour interval of 2°C; the zero contour is omitted); (b), (d), (f) precipitation (contour interval of 6 mm day^{-1}, starting at ±3 mm day^{-1}); (right) zonally averaged insolation at the top of the atmosphere (dash–dotted line; bottom x axis; units of W m^{-2}) and zonally averaged Atlantic SST (solid line; top x axis; units of °C).

Over most of the ocean, the June–March SAT anomalies due to SST are indistinguishable from the total anomalies (shown in Fig. 6), with the noticeable exception of the eastern seaboard–northwest Atlantic region, where the temperature gradient is washed out in the absence of insolation changes. The SST changes induce SAT changes well inland, but their magnitude is overall quite small: 15%–30% (depending on the estimate) of the CTL changes in northwest Africa and 50% in extratropical South America. SST also induces positive anomalies in northeast Brazil and in south-central Africa that are not present in the CTL annual cycle. The two experiments provide somewhat different estimates of the SST-induced June–March anomalies in the Guiana highlands (northern South America), the Guinea region, and the eastern Sahara. In Guiana and Guinea the negative anomalies do not reach as far north in the

PWSol run as in the PVE run; in the Sahara the PWSol run is 3°C warmer than the PVE run.

The patterns of the September–March and December–March terrestrial surface air temperature anomalies due to SST are very similar to the June–March, and only the magnitude of the anomalies changes noticeably. The September–March SST produces SAT anomalies with a pattern very similar to the CTL case—especially in the PVE run, less so in the PWSol run, in which the negative anomalies over North Africa do not extend far enough north—and 60% or more of the magnitude (cf. Figs. 7c,d with Fig. 6c). The effect of SST on the December–March changes (Figs. 7e,f) is very small, and is more than counteracted by the effect of insolation nearly everywhere (cf. Fig. 6e with Figs. 7e,f). Only along the northeastern coasts of South America (in Guiana and northeast Brazil) is the December–March change in SAT
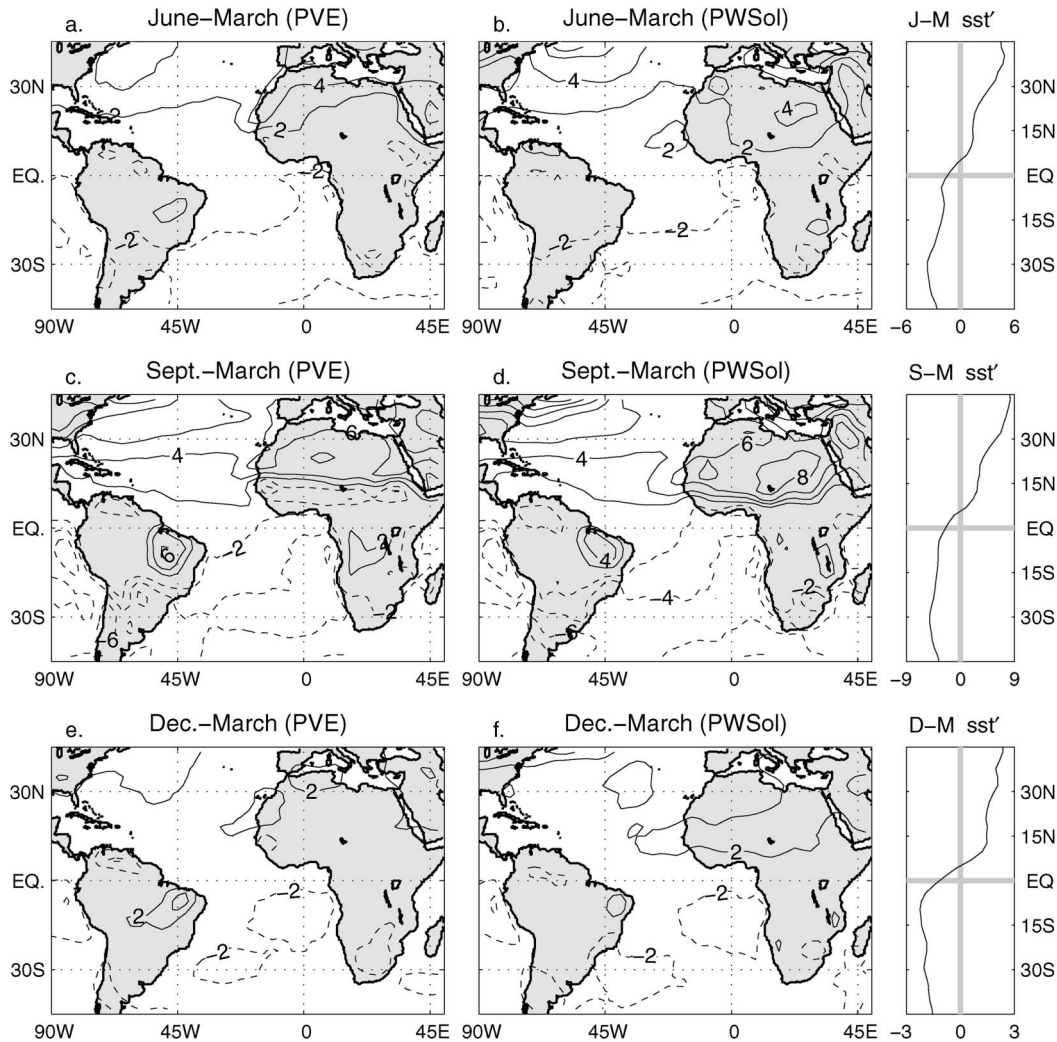
Fig. 7. The portion of the annual cycle of surface air temperature (presented as departures from the month of Mar) that can be attributed solely to seasonal changes in SST. (a), (c), (e) Estimate obtained from PVE (Mar insolation boundary conditions); (b), (d), (f) estimate obtained from PWSol (Dec insolation boundary conditions); (right) zonally averaged Atlantic SST (°C). The contour interval is 2°C in all maps; the zero contour is omitted. Land surface temperatures are affected by SST. The Sep–Mar anomalies due to SST are 60%–100% of the total seasonal changes shown in Fig. 6. SST plays a more modest role in the solstice months.

determined by SST. (Note also that in this region SAT anomalies are larger in December than in June, and that, even if the basin-averaged forcing is smaller, the anomalous SST meridional gradient in the western equatorial Atlantic is actually larger in December.) Finally, we note that the terrestrial SAT response to SST is approximately linear, in the sense that the general features of the response of the system to a given SST change are similar in the two runs, regardless of the different insolation conditions.

Figure 8 presents the portion of the annual cycle of precipitation that is due to changing SST. It is structured as Fig. 7. Over the equatorial Atlantic Ocean, the anomalous precipitation field is a north–south dipole in all months, indicating that, as anticipated in section 3, the oceanic ITCZ moves north with the warm SST in all

months (inspection of the annual cycle in the PMAS confirms that only the Atlantic SST influences the position of the Atlantic ITCZ). The fact that the anomalous precipitation dipole is roughly symmetric about the zero line indicates that, in the PVE and PWSol runs, the intensity of precipitation in the ITCZ changes little from one season to the next. The influence of SST on the rainfall of coastal regions is apparent. The positive rainfall anomalies in the north equatorial Atlantic extend into the Guiana highlands, the Caribbean, and Central America. The negative anomalies to the south extend into northeast Brazil (to 50°W in June and December, somewhat farther inland in September, when the SST anomalies are strongest). Note the correspondence between negative precipitation anomalies and positive temperature anomalies (and vice versa) in this region,
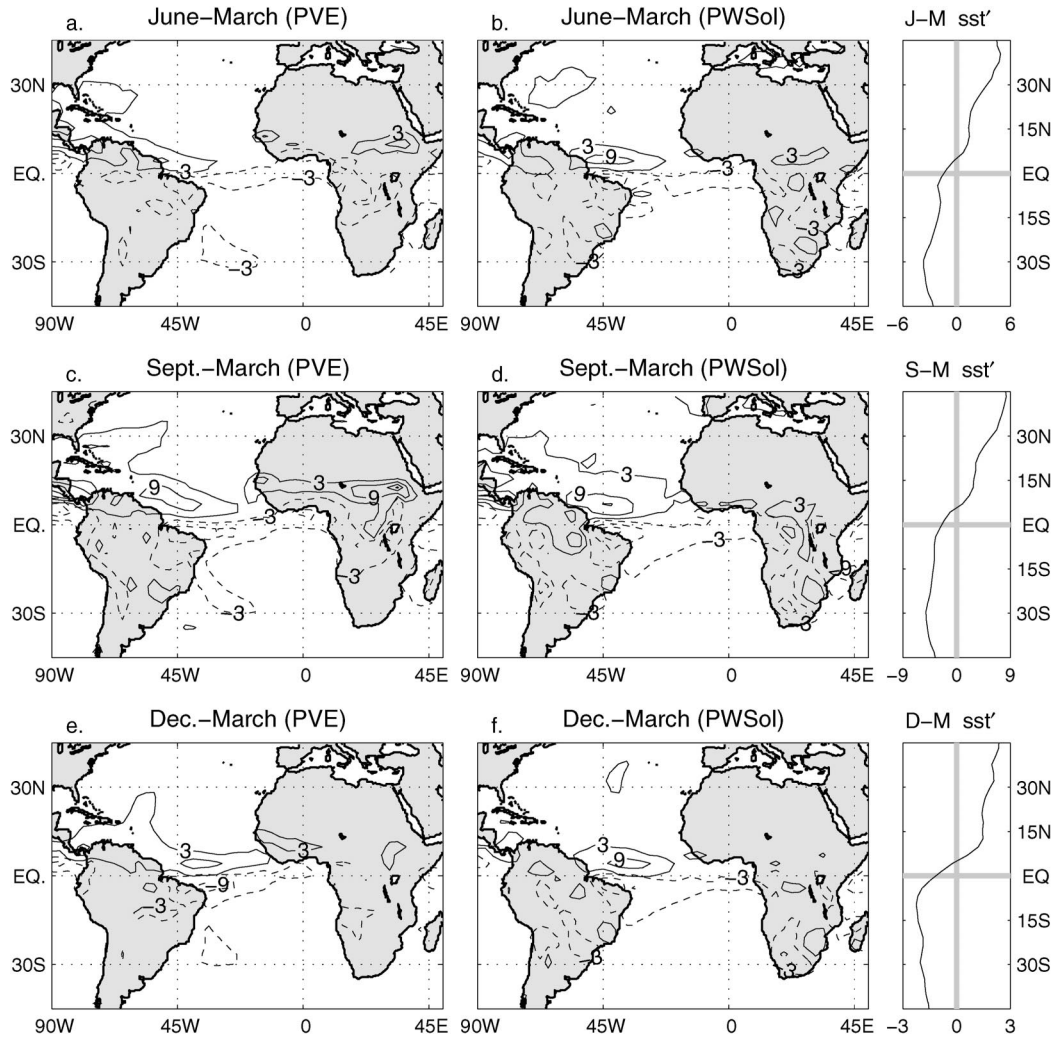
FIG. 8. The portion of the annual cycle of precipitation (presented as departures from the month of Mar) that can be attributed solely to seasonal changes in SST. (a), (c), (e) Estimate obtained from PVE (Mar insolation boundary conditions); (b), (d), (e) estimate obtained from PWSol (Dec insolation boundary conditions); (right) zonally averaged Atlantic SST (°C). The contour interval is 6 mm day^{-1} in all maps, starting at ± 3 mm day^{-1}. SST controls the position of the ITCZ. SST also affects the Guinea and Sudan regions in Africa and the Guiana highlands and northeast Brazil in South America. SST is the dominant forcing over the tropical continents in Sep.

which indicates that SAT anomalies are due to changes in cloudiness and evaporation. In equatorial Africa, the influence of SST is substantial in June and September, but limited in December.

In the PVE run, the June–March SST anomalies induce positive rainfall anomalies in eastern Sudan and negative anomalies in Guinea, the Congo basin, and the East Africa highlands; in September, the rainfall anomalies intensify and extend over the entire Sahel/Sudan region and central equatorial Africa. The general pattern of rainfall anomalies simulated by the PWSol run over tropical Africa is similar to that of the PVE run: it indicates that a positive meridional SST gradient pushes rainfall farther north into the Guinea region, intensifies it in the central equatorial Africa, and reduces it in the Congo basin and in the East Africa highlands. Never-

theless, the rainfall anomalies in the PWSol run are confined south of 10°N, and do not reproduce the strong effect of SST on the Sahel/Sudan rainfall captured by the PVE run. The PWSol run shows an influence of SST on African rainfall south of 15°S that is not reproduced in the PVE run.

6. The effect of insolation

In this section we present results from the PMS and PSS runs, in which the SST boundary conditions are held fixed, while insolation varies seasonally. We will refer to our results as to the insolation-induced anomalies. In nature all seasonal changes are ultimately caused by the seasonal changes in insolation. In our simulations, instead, the state of the ocean is not mod-
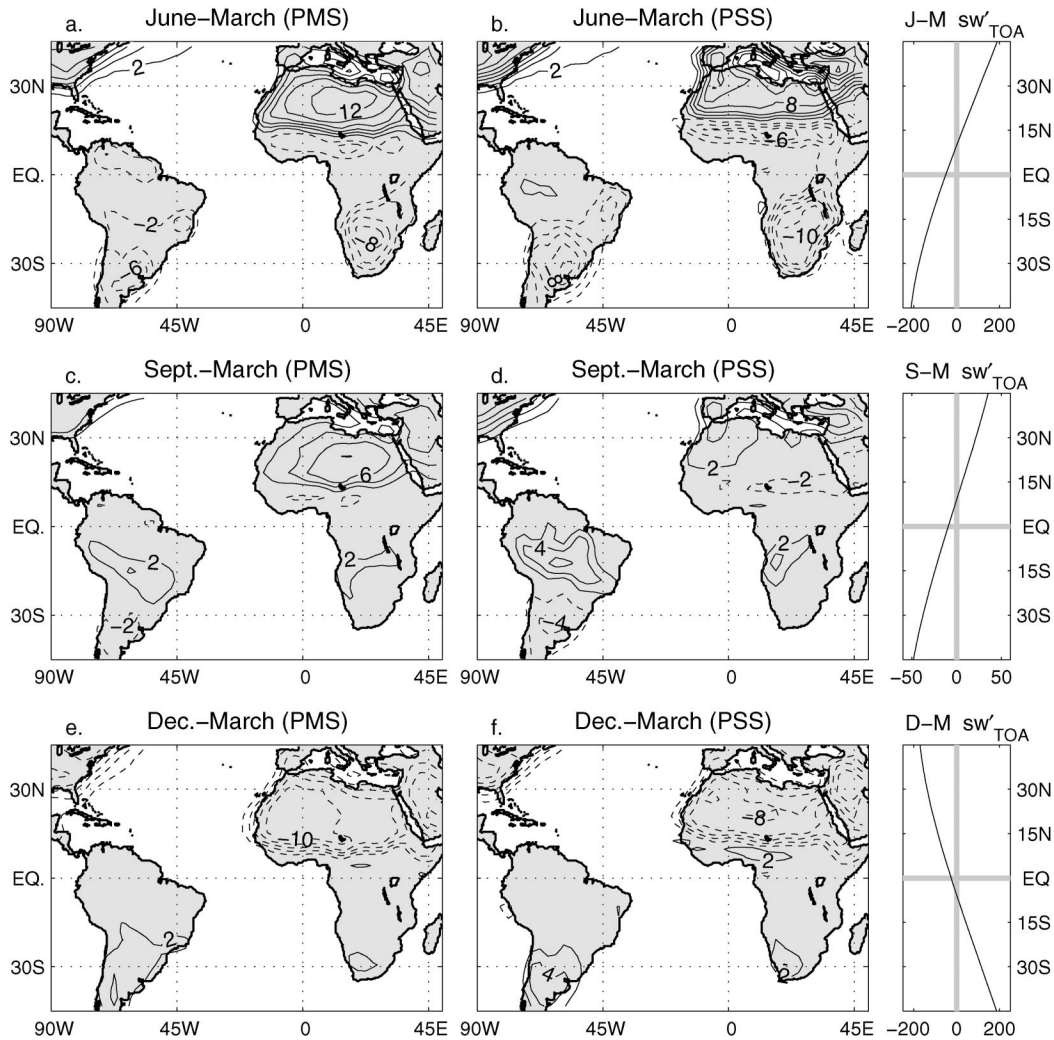
FIG. 9. The portion of the annual cycle of surface air temperature (presented as departures from the month of Mar) that can be attributed solely to seasonal changes in insolation. (a), (c), (e) Estimate obtained from PMS (Mar SST boundary conditions); (b), (d), (f) estimate obtained from PSS (Sep SST boundary conditions); (right) zonally averaged insolation at the top of the atmosphere (W m^{-2}). The contour interval is 2°C in all maps; the zero contour is omitted. Insolation alone suffices to determine the bulk of land surface temperature changes in Jun and Dec.

eled, but is prescribed as a boundary condition, thus, insolation does not affect SSTs. Therefore when we say "insolation-induced anomalies" we mean it as a shorthand for "changes that are a direct response of the land–atmosphere system to changes in insolation, and that are not mediated by changes in the ocean surface temperature."

Figure 9 presents the portion of the SAT annual cycle due to insolation, along with the zonally averaged insolation forcing. Comparison with Fig. 6 confirms that insolation is the dominant forcing during the solstice months for SAT over both the landmasses and the western North Atlantic, in the Gulf Stream region. Insolation-induced SAT anomalies in Fig. 9 are typically 60%–100% of the total change shown in Fig. 6.

Figures 9a and 9b represent two estimates of the in-

solation-induced June–March anomalies associated with fixed March and September SST boundary conditions, respectively. The general pattern is quite similar in the two maps, but there are many small but interesting differences. For example, the SAT anomalies outside the deep Tropics have smaller magnitude in PMS than in PSS and the negative anomalies in the Sahel region is weaker and displaced farther south. This suggests that, in this region, SAT anomalies are not generated as a direct response to insolation; in fact, differences between SAT anomalies in the Sahel in the PMS and PSS are reproduced in differences in the precipitation anomalies (see Fig. 10).

The two estimates of the SAT response to September–March insolation changes shown in Figs. 9c,d reproduce the coarser features of the control September–March
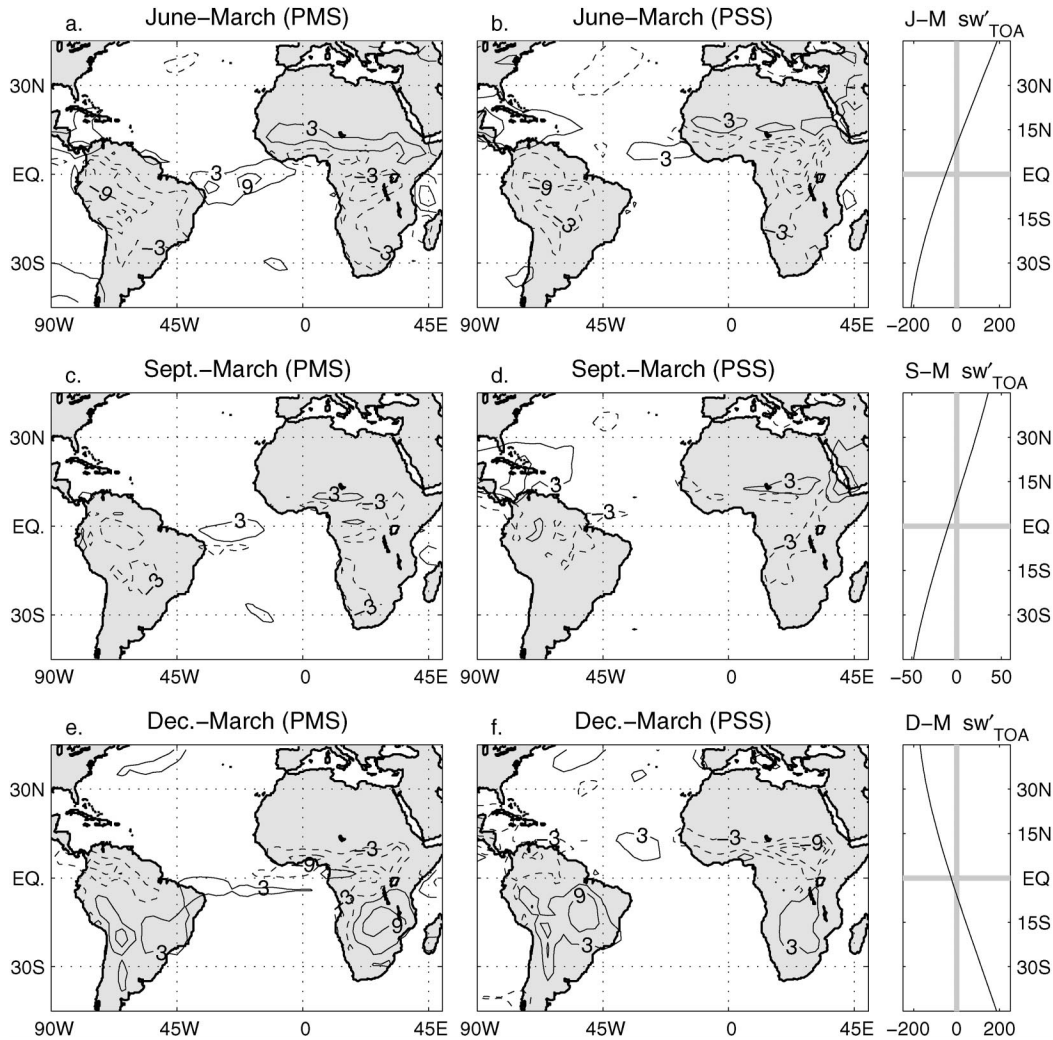
FIG. 10. The portion of the annual cycle of precipitation (presented as departures from the month of Mar) that can be attributed to seasonal changes in insolation. (a), (c), (e) Estimate obtained from PMS (Mar SST boundary conditions); (b), (d), (f) estimate obtained from PSS (Sep SST boundary conditions); (right) zonally averaged insolation at the top of the atmosphere (W m^{-2}). The contour interval is 6 mm day^{-1} in all maps, starting at ± 3 mm day^{-1}. Insolation controls the position of continental convection in Jun and Dec, and modulates the intensity of oceanic convection during all months.

changes (Fig. 6c), but are generally smaller. Moreover, the two estimates are quite different from each other, and where one experiment produces sizable anomalies (North Africa in the PMS, Brazil in the PSS), the other does not. This behavior is consistent with a minor role of insolation in determining land surface temperature in September (cf. Fig. 6c with Figs. 9c,d) and the predominance of SST established in section 5 (cf. Fig. 6c with Figs. 7c,d).

As expected, the December–March SAT differences are produced by the changes in insolation almost everywhere over the continents. Notable exception are found only in the coastal regions of equatorial South America and South Africa, where SST produces sizable anomalies with the same sign of the CTL (cf. Fig. 6e with Figs. 7e,f and Figs. 9e,f). The two estimates of the

insolation-induced anomalies shown in Figs. 9e,f are quite similar.

Figure 10 presents the portion of the rainfall seasonal changes due to insolation, along with the zonally averaged insolation forcing. By comparing Fig. 10 to Fig. 6 (right), we can conclude that (i) the bulk of the June–March and December–March anomalies over the continents is captured by imposing changes in insolation; (ii) for the September–March anomalies, insolation has a robust and dominant effect only in South Africa; and (iii) there is a sizable influence of insolation on the intensity of the oceanic precipitation. It is important to note that precipitation anomalies over the tropical Atlantic Ocean are produced only where there is significant precipitation in the basic state. When the basic state has March SST boundary conditions (PMS run; Figs.

10a,c,e), the precipitation anomalies over the ocean are confined to the equator. When the basic state has September SST boundary conditions, (PSS run; Figs. 10b,d,f) the largest precipitation anomalies over the ocean are in the Caribbean and the Gulf of Mexico. During June and December there is an additional precipitation anomaly in the central Atlantic, at about 10°N. Precipitation anomalies, whether they are positive or negative, are colocated with the ITCZ of the basic state. Therefore this coincidence cannot be solely attributed to the fact that precipitation is a positive definite variable. While the position of the ITCZ is largely established by coupled atmosphere–ocean interactions (ultimately also paced by insolation), the circulation induced over the continental landmasses by changing insolation extends over the oceanic regions and greatly affects the intensity of oceanic convection.

7. Statistical significance and nonadditive effects

The previous two sections showed the SAT and precipitation responses to seasonal variation in SST and solar forcing. The responses were inferred by looking at the annual variations in experiments where the annual cycle of one of the two forcings had been suppressed. This method has the advantage of presenting the actual pattern of the response: for example, it indicates that the SST-induced northward shift of the ITCZ between March and September is associated with a 4°C warming of northeast Brazil and a 2°C cooling in the Guiana highlands. The disadvantage of the method is that it does not gauge the statistical significance of the response, and can only provide a qualitative indication of nonlinear interactions existing between insolation and SST when they act together in generating the control annual cycle. The analysis of variance (anova; Von Storch and Zwiers 1999) is the appropriate statistical tool to investigate questions of significance and nonadditivity of the responses.

The CTL, PMS, PVE, and PM runs form a complete set of experiments in which the two factors whose effect we are set out to prove—that is, the presence or absence of an annual cycle of insolation and the presence or absence of an annual cycle of SST—are combined in all possible ways (or "treatments"). In CTL, SST and insolation are annually varying; in PMS, SST is constant at the March value and insolation is annually varying; in PVE, SST is annually varying and insolation is constant at the March value; in PM, both SST and insolation are constant at the March value. Every year of a model integration can be considered as a member of an ensemble of experiments subject to the same treatment. Thus we have four eight-member ensembles.

Let us assume, for example, that we want to measure the effects of the SST treatment and insolation treatment on the June precipitation. For every June of any of the four experiments, we can write

$$P = \overline{P} + P_I + P_S + P_{IS} + \varepsilon,$$

where $\overline{P}$ is the baseline, that is, the grand mean of all June months in the four experiments; P_I represents the departure from the baseline due to the effect of insolation; P_S represents the departure due to the effect of SST; P_{IS} represents the departure due to the effect of interactions between insolation and SST treatments; and, finally, ε represents random interannual variability.

If annual variations of neither SST nor insolation had any effect, June would look the same, aside from random variability, in all experiments (it would look a lot like March, in our setup), and P_I, P_S, and P_{IS} would all be statistically indistinguishable from zero. This is the null hypothesis that can be tested with the anova technique.

Figures 11 and 12 show where the effects of SST, of insolation, and of their nonadditive interaction are significant at the 95% level in producing the annual cycle of SAT and precipitation. In this setup, "producing the annual cycle" is tantamount to say "making June, September, and December different from March." Therefore Figs. 11 and 12 indicate that the anomalies discussed in sections 5 and 6 are significant. Moreover, they confirm what was inferred by comparing PMS to PSS and PVE to PWSol, that is, the existence of interactions between SST and insolation treatments in the ITCZ region, the Sahel, and northern South America.

8. Summary and discussion

This paper describes a set of GCM experiments performed with CCM3 and intended to elucidate the relative role of changes in SST and insolation over land in producing the annual cycle of surface air temperature and precipitation over the tropical Atlantic, Africa, and South America. The simulated CTL annual cycle replicates the general characteristics of the observed annual cycle, but there are substantial biases; in particular, the amount of continental precipitation is grossly overestimated by CCM3.

We have presented results from four modeling studies (PVE, PWSol, PMS, and PSS; see Table 1) designed to distinguish what portion of the annual cycle of temperature and precipitation is due to a direct response of the land–atmosphere system to seasonal changes in insolation, and what portion is a response to changes in SST. In the PVE and PWSol runs the insolation at the top of the atmosphere is held fixed at the boreal vernal equinox and winter solstice values, respectively, while the SST is allowed to vary according to the observed climatology. Therefore, comparison of two months extracted from the climatology of either the PVE or the PWSol run provides an estimate of the effect of SST changes. In the PMS and PSS runs the SST boundary conditions are held fixed at March and September values, respectively, while insolation changes. Therefore, the climatologies of the PMS and PSS runs reveal the

SAT

June – Factor:SST   June – Factor:Insolation   June – Interaction

Sept. – Factor:SST   Sept. – Factor:Insolation   Sept. – Interaction

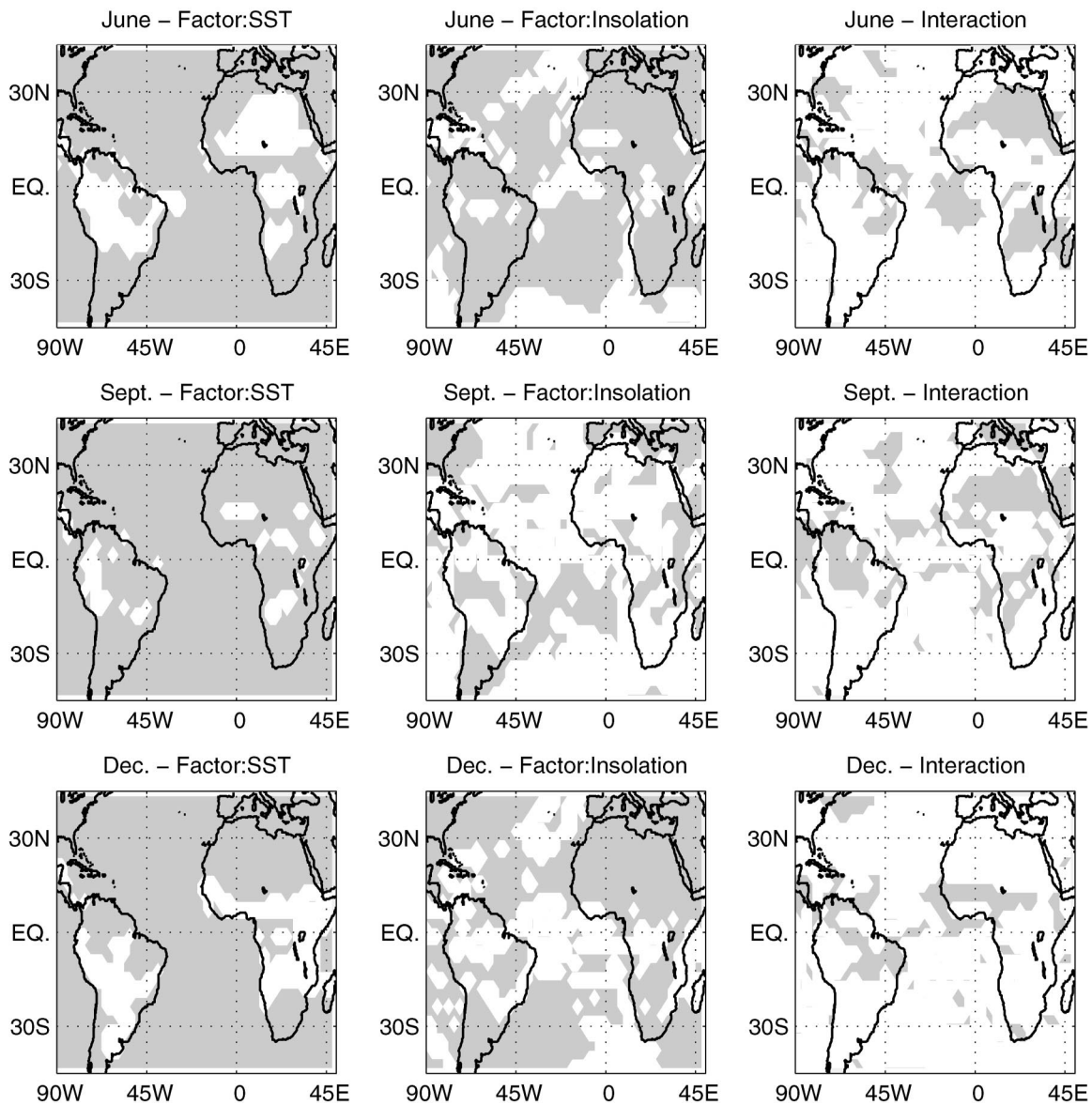Dec. – Factor:SST   Dec. – Factor:Insolation   Dec. – Interaction

FIG. 11. Regions where (left) SST, (center) insolation, and (right) their interaction contribute significantly (at the 95% level) in making SAT values during Jun, Sep, and Dec different from SAT values in perpetual Mar conditions.

direct response of the land–atmosphere system to insolation. The degree to which estimates obtained by the PVE and PWSol (PMS and PSS) runs differ gives a qualitative measure of the linearity of the response to SST (insolation) changes

Figure 13 gives an estimate of the relative role of SST annual variations, insolation annual variations, and their interactions. The annual signal of a variable [surface air temperature (SAT) or precipitation] is represented by its total variance minus the variance due to random fluctuation, and it can be expressed as the sum

of the variance due to the SST treatments, the insolation treatments, and their interactions. The ratios of the factor- and interaction-induced variances to the annual signal are plotted in Fig. 13 by increments of 25% (the contour line indicates the 50% value). Although the significance of these ratios is not established, we find them to be a useful guide in summarizing our results.

SST is the dominant forcing for the terrestrial SAT in northeast South America (the Guiana highlands and northeast Brazil), the Gulf of Guinea, the Congo basin, and South Africa. The direct response to insolation
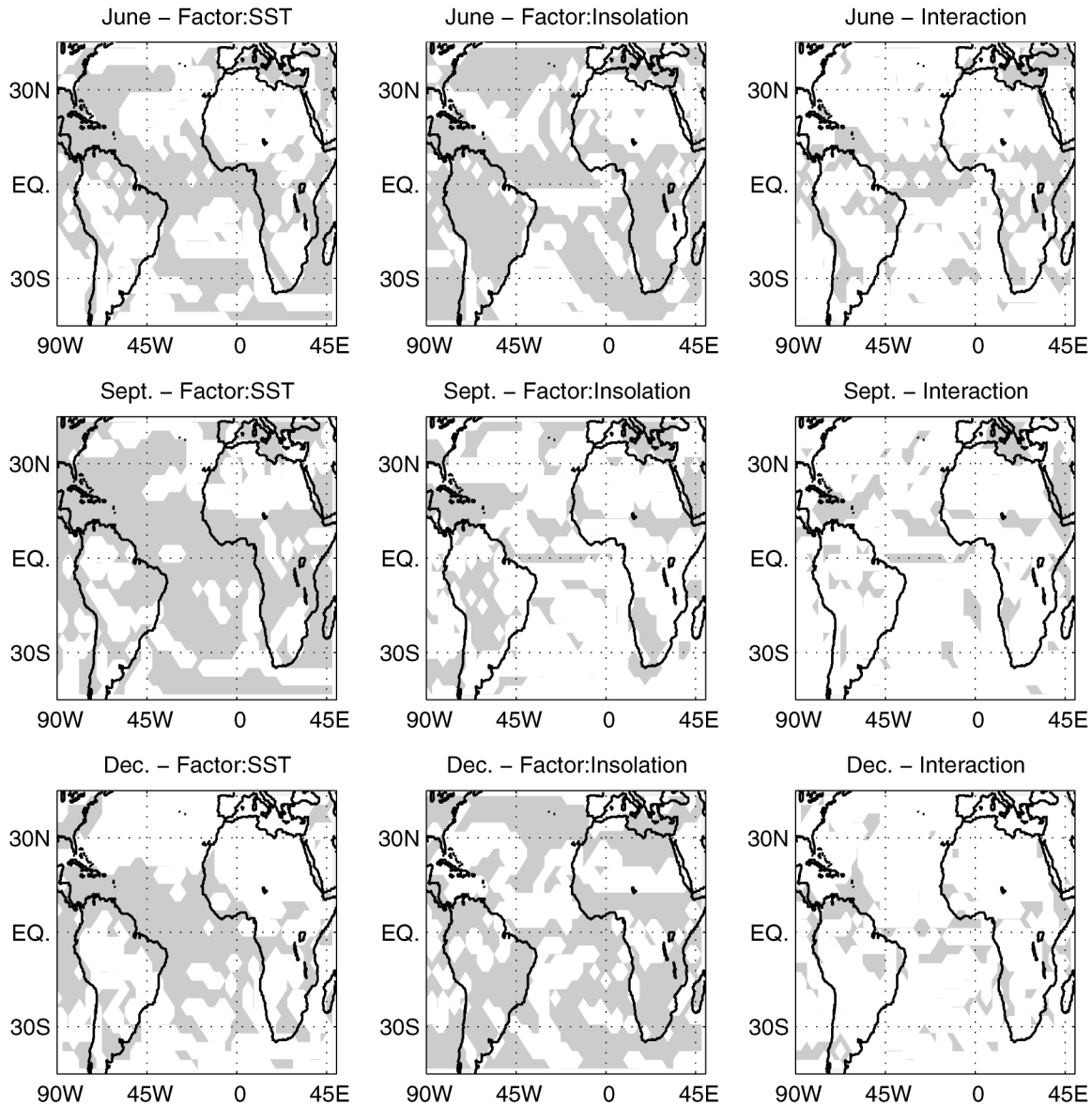
PRECIPITATION

FIG. 12. Regions where (left) SST, (center) insolation, and (right) their interaction contribute significantly (at the 95% level) in making precipitation values during Jun, Sep, and Dec different from precipitation values in perpetual Mar conditions.

anomalies explains the greatest part of the annual cycle of SAT over land outside the deep Tropics (and except the southern tip of Africa).

Maritime precipitation in the Tropics responds most strongly to SST changes (the location of the ITCZ shifts to follow closely the warmest waters). SST changes also account for the bulk of the annual cycle in precipitation over the Guiana highlands, northeast Brazil, and the Gulf of Guinea region. The SST impact on precipitation over the Sahel is on average between 25% and 50%. The direct response of land to changes in insolation is responsible for the bulk of seasonal changes in precip-

itation over Africa and South America. The effect of insolation variations on the equatorial Atlantic precipitation is between 25% and 50%: the insolation-induced anomalies over land drive circulation anomalies that extend over the ocean and significantly affect the intensity, but not the location, of maritime precipitation.

The interaction between SST and insolation, although significant in a larger portion of the domain, accounts for more than 25% of the total annual signal only in a small portion of the domain, which includes the Sahel.

Although the subject of this paper is the annual cycle, we believe that two additional conclusions regarding the
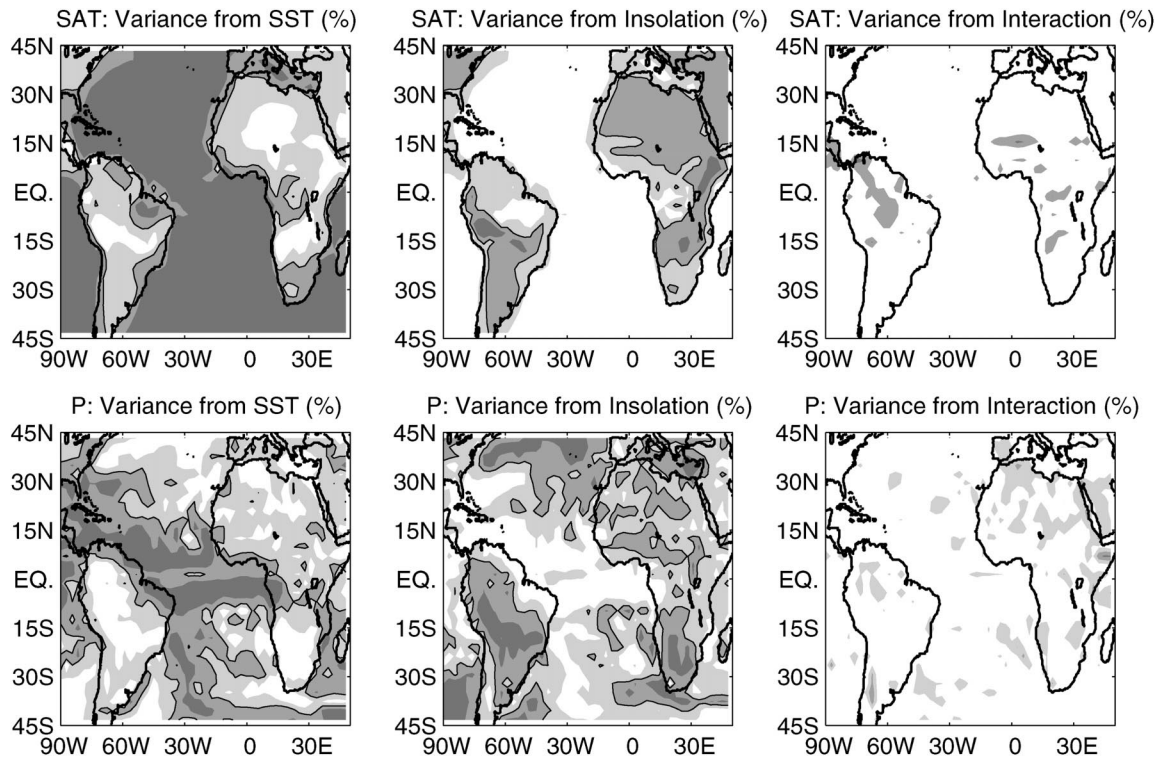
FIG. 13. Percentage of the annual variations in (top) SAT and (bottom) precipitation that can be ascribed to (left) SST, (center) insolation, and (right) their interaction. Darker gray shading indicates a larger percentage of explained annual variations (the increment equals 25%); the solid line is the 50% contour.

interannual climate variability in the tropical Atlantic region are warranted. (i) We have shown that SST is an important forcing of the annual cycle of precipitation in the same regions where it is an important forcing of interannual precipitation variability, namely, northeast Brazil, Gulf of Guinea, Sudan, and Sahel (e.g., Nobre and Shukla 1996; Rowell et al. 1995). This finding suggests that the same mechanisms might be at play in shaping both the annual cycle and the interannual variability, and that we can indeed gain some understanding of the variability by examining the much larger signal in the annual cycle. (ii) The presence of a large but nonlinear response of oceanic precipitation to insolation forcing over land suggests that a linear analysis of tropical Atlantic variability, or an analysis not stratified by season, might fail to fully capture a substantial effect of land processes.

Conclusions regarding the nonlinearity of the response in our experiments should take into account the following caveats. (i) Identical mean changes can be accomplished by different physical processes, thus our limited analysis cannot prove true linearity. (ii) The PVE and PWSol runs and the PMS and PSS runs differ not only in insolation and SST, respectively, but also in soil moisture, which is calculated by the land surface model; because of the long memory of the soil, soil moisture anomalies are both a response to and a forcing for the atmospheric conditions, and their contribution to the

nonlinearity of the atmospheric response cannot be separated in the current setup.

We conclude this discussion by acknowledging the limits of our current approach. In choosing to analyze the annual cycle of air temperature and precipitation as a response to two independent forcings, insolation and SST, we have obviously chosen a workable decomposition while neglecting some basic physics: both the direct response of the ocean to insolation and the effect of ocean–atmosphere coupling have been consciously overlooked. We plan to couple the atmospheric model to a slab ocean model and perform experiments analogous to those presented in this paper. A terrestrial influence on SST will then be possible, although the coupling with ocean dynamics will still be neglected.

A dynamical explanation of the mechanisms that link temperature and precipitation over land to temperature and precipitation over the ocean is also much needed, and will be the subject of a future paper.

Atmospheres as a contribution to the GEWEX Global Precipitation Climatology Project. The NCEP reanalysis data were provided by the NOAA–CIRES Climate Diagnostics Center, Boulder, Colorado, from their Web site at http://www.cdc.noaa.gov/.

REFERENCES

Bonan, G. B., 1996: A land surface model (LSM version 1.0) for ecological, hydrological, and atmospheric studies: Technical description and user's guide. Tech. Rep. NCAR/TN-417+STR, NCAR, 150 pp.

——, 1998: The land surface climatology of the NCAR Land Surface Model coupled to the NCAR Community Climate Model. *J. Climate,* **11,** 1307–1326.

Braconnot, P., O. Marti, S. Joussame, and Y. Leclainche, 2000: Ocean feedback in response to 6 kyr BP insolation. *J. Climate,* **13,** 1537–1553.

Carton, J. A., and Z. Zhou, 1997: Annual cycle of sea surface temperature in the tropical Atlantic Ocean. *J. Geophys. Res.,* **102** (C13), 27 813–27 824.

Dickinson, R. E., A. Henderson-Sellers, and P. J. Kennedy, 1993: Biosphere–Atmosphere Transfer Scheme (BATS) Version 1e as coupled to the NCAR Community Climate Model. Tech. Rep. NCAR/TN-387+STR, NCAR, 72 pp.

Eltahir, E. A. B., and C. Gong, 1996: Dynamics of wet and dry years in West Africa. *J. Climate,* **9,** 1030–1042.

Folland, C. K., T. N. Palmer, and D. Parker, 1986: Sahel rainfall and worldwide sea temperature. *Nature,* **320,** 602–687.

——, A. W. Colman, D. P. Rowell, and M. K. Davey, 2001: Predictability of Northeast Brazil rainfall and real-time forecast skill, 1987–98. *J. Climate,* **14,** 1937–1958.

Fu, R., R. E. Dickinson, M. Chen, and H. Wang, 2001: How do tropical sea surface temperatures influence the seasonal distribution of precipitation in the equatorial Amazon? *J. Climate,* **14,** 4003–4026.

Hack, J., J. Kiehl, and J. Hurrell, 1998: The hydrologic and thermodynamic characteristics of the NCAR CCM3. *J. Climate,* **11,** 1207–1236.

Huffman, G. J., and Coauthors, 1997: The Global Precipitation Climatology Project (GPCP) Combined Precipitation Data Set. *Bull. Amer. Meteor. Soc.,* **78,** 5–20.

Hurrell, J., J. Hack, B. Boville, D. Williamson, and J. Kiehl, 1998: The dynamical simulation of the NCAR Community Climate Model Version 3 (CCM3). *J. Climate,* **11,** 1207–1236.

Kalnay, E., and Coauthors, 1996: The NCEP/NCAR 40-Year Reanalysis Project. *Bull. Amer. Meteor. Soc.,* **77,** 437–471.

Kiehl, J. T., J. J. Hack, G. B. Bonan, B. A. Boville, D. L. Williamson, and P. J. Rasch, 1998: The National Center for Atmospheric Research Community Climate Model: CCM3. *J. Climate,* **11,** 1131–1150.

Li, T., and S. G. H. Philander, 1997: On the seasonal cycle of the equatorial Atlantic. *J. Climate,* **10,** 813–817.

Mitchell, T. P., and J. M. Wallace, 1992: The annual cycle in equatorial convection and sea surface temperature. *J. Climate,* **5,** 1140–1156.

Nobre, P., and J. Shukla, 1996: Variations of sea surface temperature, wind stress, and rainfall over the tropical Atlantic and South America. *J. Climate,* **9,** 2464–2479.

Parker, D. E., C. K. Folland, A. Bevan, M. Ward, M. Jackson, and K. Maskell, 1996: Marine surface data for analysis of climatic fluctuations on interannual to century timescales. *Natural Climate Variability on Decade-to-Century Timescales,* D. G. Martinson et al., Eds., National Academy Press, 241–250.

Philander, S. G. H., D. Gu, D. Halpern, G. Lambert, N.-C. Lau, T. Li, and R. Pacanowski, 1996: Why the ITCZ is mostly north of the equator. *J. Climate,* **9,** 2958–2971.

Reynolds, R. W., and T. M. Smith, 1994: Improved global sea surface temperature analyses. *J. Climate,* **7,** 929–948.

Rowell, D. P., C. K. Folland, K. Maskell, and M. N. Ward, 1995: Variability of summer rainfall over tropical North Africa (1906–92): Observations and modelling. *Quart. J. Roy. Meteor. Soc.,* **121,** 669–704.

Shea, D. J., K. E. Trenberth, and R. W. Reynolds, 1992: A global monthly sea surface temperature climatology. *J. Climate,* **5,** 987–1001.

Shukla, J., and M. Fennessy, 1994: Simulation and predictability of monsoons. Proceedings of the International Conference on Monsoon Variability and Prediction, Tech. Rep. WCRP-84, World Climate Research Program, Geneva, Switzerland, 567–575.

Uvo, C. B., C. A. Repelli, S. Zebiak, and Y. Kushnir, 1998: The relationships between tropical Pacific and Atlantic SST and northeast Brazil monthly precipitation. *J. Climate,* **11,** 551–562.

von Storch, H., and F. W. Zwiers, 1999: *Statistical Analysis in Climate Research.* Cambridge University Press, 484 pp.

Ward, M. N., 1998: Diagnosis and short-lead time prediction of summer rainfall in Tropical North Africa at interannual and multidecadal timescales. *J. Climate,* **11,** 3167–3191.

Werner, K., 1999: Natural variability of the tropical Atlantic climate system. M.S. thesis, University of Washington, 95 pp.

Xie, S. P., and S. G. H. Philander, 1994: A coupled ocean–atmosphere model of relevance to the ITCZ in the eastern Pacific. *Tellus,* **46A,** 340–350.